JOURNAL OF CATALYSIS 134, 98–106 (1992)

A Stable Catalyst for Heavy Oil Processing

II. Preparation and Characterization

C. GALARRAGA AND M. M. RAMÍREZ DE AGUDELO

INTEVEP, S. A. Catálisis Aplicada, Apdo. 76343, Caracas, Venezuela

Received January 3, 1991; revised September 27, 1991

The hydroprocessing of heavy oils is a complex task. The high contaminant content of these oils causes poisoning and rapid deactivation of the catalysts commonly employed. Since iron-containing catalysts, namely bauxites and laterites, have been demonstrated to possess remarkable activity for hydrodemetallization reactions, two series of $FeMo/Al_2O_3$ catalysts have been prepared and characterized. In order to improve both hydrodesulfurization and hydrogenation activity, molybdenum was included in the catalyst formulation. The preparation was carried out by successive impregnation of the support. α-Fe_2O_3, γ-Fe_2O_3, α-$FeMoO_4$, and β-$FeMoO_4$ were identified in the precursor catalysts by X-ray diffraction. The sulfided samples exhibited two phases: Fe_7S_8 in hexagonal structure and $Fe_xMo_yS_z$. Mössbauer spectroscopic studies of sulfided samples confirmed the presence of the $Fe_xMo_yS_z$ phase, which contains two types of Fe^{2+} sites (I and II). Site I corresponds to a tetrahedral coordination and site II was found to be octahedral.

INTRODUCTION

Heavy oils typically contain high amounts of metal, nitrogen, and sulfur. These contaminants poison and rapidly deactivate the conventional hydrotreatment catalysts. Their processing is a complex task. Hence, the development of new catalysts more active during metal deposition is of great importance in catalysis.

Studies on hydroprocessing have been centered mainly on hydrodesulfurization (HDS) reactions and their catalysts. Various surface models have been proposed for the active phase (*1*). The hydrodemetallization (HDM) and hydrodenitrogenation (HDN) reactions have not been studied as deeply as the HDS reaction.

Generally, the literature published on HDM reactions stresses the need for an extensive macroporosity in the catalyst. The large pores are needed to allow the access of high-molecular-weight species and to prevent pore blockage and consequent deactivation (*2*). On the other hand, a bifunctional catalyst that consists of a solid acid carrier and a phase able to exchange hydrogen is regarded as ideal for HDN reactions (*3*).

The catalysts commonly employed in hydroprocessing have been based on combinations of metals of Group VIII and Group VIB of the periodic table, i.e., Co, Ni, Fe, Mo, and W supported on Al_2O_3, SiO_2 and SiO_2–Al_2O_3. Regarding the use of Fe, it has been demonstrated that bauxites and laterites have remarkable catalytic properties in the HDM reaction (*4*). In addition, the attractive cost of naturally occurring catalysts has prompted us to study Fe-based catalysts.

The present work is part of a systematic study that includes the design, preparation, and characterization of a series of FeMo-type catalysts, as well as their evaluation for reactions of heavy oil processing. In Part I (*5*), we have considered the methodology and concepts used to achieve the development of this new type of catalyst (*6*). The preparation methods and their effect on the final structure of the catalyst are detailed

0021-9517/92 $3.00

below. Activity and selectivity for the different reactions involved in the hydroprocessing of heavy oils are discussed in Part III (*7*). Finally, the correlations between observed phases and activity and selectivity are reported in Part IV (*8*).

X-ray diffraction (XRD) and Mössbauer spectroscopy have been used for the characterization of the catalysts in order to identify the phases present. Mössbauer spectroscopy was used to identify the chemical nature of the Fe sites and their interactions with the support and the Mo sites. Also it assisted us in understanding the role of each of them and also the stability exhibited by some of the catalysts when they are employed in hydroconversion reactions.

Currently the two modes of using Mössbauer spectroscopy, namely absorption and emission, have been employed in the characterization of hydrotreatment catalysts (*9*). Doping ^{57}Fe or using ^{57}Co in Co–Mo catalysts has led to controversial results. The so-called aftereffects (*10*) are partially responsible for misinterpretations. Fe and Co not only have different chemical and electronic properties but also the stable state of Fe may be different from that of Co. Moreover, the decay of ^{57}Co may create unstable and very different ^{57}Fe species. The Mössbauer spectra of Fe–Mo sulfided catalysts were observed to be very similar to those of Co–Mo sulfided catalysts (*11*). Thus the Q_1 doublet (*11*, Fig. 26) observed for $FeMo/Al_2O_3$ catalysts appears to be caused by the presence of a quite analogous Co–Mo–S phase, i.e., the Fe–Mo–S phase.

EXPERIMENTAL

Two series of $FeMo/Al_2O_3$ catalysts were prepared by sequential impregnation, using ammonium heptamolybdate, iron nitrate, and a commercial γ-alumina (Akzo 1.5 E). A design concept of considering each metal as an active phase (in a high content) or as a promoter (low content) was followed for each series. The catalysts were designated using A for alumina, F for Fe, and M for Mo; the order of the letters F and M indicates the impregnation sequence. The designation includes also a number that represents the nominal weight percentage of the promoter. Thus, for instance, AFM-2 would be an alumina-supported catalyst in which Fe was impregnated in a first step and 2% of Mo was nominally impregnated in a second step. For all catalysts the metal in the higher content was impregnated in the first step. Series 1 (AFM) contains four catalysts in which iron was impregnated as active metal (8 wt%) and molybdenum as promoter metal (1–4 wt%). The conceptual design for catalysts of series 2 (AMF) was the reverse, with Mo content of 6 wt% and Fe ranging from 1 to 4 wt%.

For the AFM series, first the support was impregnated with an acid iron nitrate solution. The catalyst was then filtered, dried, and finally calcined at 500°C for 16 h. Then, molybdenum was impregnated using a basic ammonium heptamolybdate solution followed by filtering, drying, and calcining at 500°C for 16 h. For the AMF catalysts the procedure was the same but the steps were inverted. The catalysts were studied in their oxide and sulfide forms. The catalysts were sulfided in a cell that could be sealed under vacuum after sulfidation, by using a mixture of H_2/H_2S (10 : 1) at 350°C for 3 h. The sulfided catalysts were then handled in a dry box in order to mount them in the sealed sample holders for XRD and Mössbauer analysis.

The iron and molybdenum contents in the calcined solids were determined by atomic absorption. The physical properties of surface area, pore volume, and pore size distribution were evaluated using standard methods of nitrogen adsorption–desorption isotherms and by penetration of helium and mercury.

The XRD patterns of the samples were performed with a PW/1410/20/80 Philips diffractometer using Zr-filtered Mo$K\alpha$ radiation. The precursor catalysts were analyzed in a standard goniometer at atmospheric pressure. The sulfided samples were analyzed in a powder camera of the Debye–Scherrer type, using asymmetric as-

TABLE 1

Chemical and Physical Properties of FeMo Catalysts

Catalyst	Chemical composition Fe (wt%)	Mo (wt%)
AFM-1	8.6	1.1
AFM-2	8.5	2.2
AFM-3	8.2	3.0
AFM-4	8.1	4.0
AMF-1	2.4	6.1
AMF-2	2.8	6.6
AMF-3	4.0	6.3
AMF-4	5.0	5.9
	Physical properties	
	Series AFM (AFM-1–AFM-4)	Series AMF (AMF-1–AMF-4)
Surface area ($m^2\ g^{-1}$)	166–145	169–151
Pore volume V_p ($cm^3\ g^{-1}$)	0.88–0.81	0.87–0.82
Pore size distribution (% V_p)		
Diameter (Å)		
<90	7.8–7.2	7.4–8.0
90–300	75.5–73.1	76.1–71.4
300–500	14.4–12.5	12.8–16.7
>500	2.4–7.2	3.7–3.1

sembling of the film and an exposure time of 5 h.

The sulfided catalysts were analyzed by Mössbauer spectroscopy using ^{57}Co in palladium radiation. The spectra were obtained in numeric mode (counts per channel) and adjusted by computer. The adjusted parameters are the isomer shift (IS), the linewidth at medium height, the line intensity, the quadrupole splitting (QS), and the magnetic field (H).

RESULTS AND DISCUSSION

Quantitative Analysis and Physical Properties

The chemical and physical properties of the catalysts of the AFM and AMF series are summarized in Table 1. The results obtained from the chemical analysis indicate that all AFM catalysts fit the conceptual design. It also demonstrates that the method employed for the preparation was adequate to obtain the required metal concentration. However, the catalysts of the AFM series contain more Fe than was originally intended. The deviation was as high as about 1 wt% Fe for the last three catalysts of this series, which might indicate that the interaction of Fe with a Mo/Al_2O_3 catalyst is stronger than that existing between Fe and pure γ-Al_2O_3.

The physical properties were evaluated for the catalysts corresponding to the extremes of the series. Since the measured parameters were almost constant through the series and only a slight decrease of less than 10% was observed, we did not consider it necessary to evaluate these properties for the other catalysts. The surface area value is approximately 150 $m^2\ g^{-1}$ with a pore volume of 0.8 $cm^3\ g^{-1}$. The pore size distribution was found to range mainly in the meso-macropore size.

X-Ray Diffraction

Figure 1 shows typical X-ray diffraction patterns of the oxide catalysts and Table 2

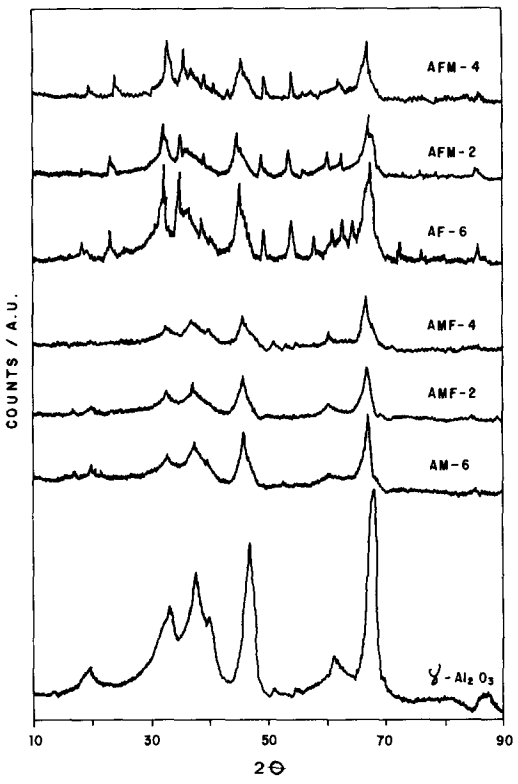

FIG. 1. XRD patterns for oxides.

summarizes the identified phases. Although the intensities of the patterns were not very strong the identification of the phases present in the catalysts in their oxide and sulfide forms was relatively simple. Table 3 collects the *d*-spacings derived from the main peaks observed in the XRD patterns of the sulfided

TABLE 2

XRD Analysis, Oxides

Catalyst	Fe/Mo	Phase 1	Phase 2
AFM-1	8.0	α-Fe_2O_3	α-$FeMoO_4$
AFM-2	3.9	γ-Fe_2O_3	α-$FeMoO_4$
AFM-3	2.8	γ-Fe_2O_3	α-$FeMoO_4$
AFM-4	2.0	γ-Fe_2O_3	α-$FeMoO_4$
AMF-4	0.9	—	α-$FeMoO_4$
AMF-3	0.7	α-Fe_2O_3	α-$FeMoO_4$
AMF-2	0.4	α-Fe_2O_3	α-$FeMoO_4$
AMF-1	0.3	α-Fe_2O_3	β-$FeMoO_4$

TABLE 3

XRD Analysis, *d*-Spacings for Oxides

Catalyst	*d* (Å)		
AF-6	2.639	2.079	1.724
AFM-2	2.640	2.240	1.701
AFM-4	2.688	2.268	1.694
AM-6	2.673	2.277	1.644
AMF-2	2.710	2.275	1.638
AMF-4	2.733	2.269	1.636

catalysts. The aim of this study was to work out the effect of the promoter metal on inducing the formation of any new phase. We have grouped the observed phases as phase 1 (a single metal oxide) and phase 2 (a mixed oxide).

α-Fe_2O_3, γ-Fe_2O_3, and α-$FeMoO_4$ were found for the AFM series, while the AMF series presented the α-form of iron oxide and mainly α-$FeMoO_4$, except AMF-1 in which β-$FeMoO_4$ was observed instead.

A graphical representation of the phase 1/phase 2 ratio vs the atomic Fe/Mo ratio is presented in Fig. 2. These results revealed a significant dependence of the phase ratio on the Fe/Mo ratio in the catalyst. The phase ratio for the AFM series was found to increase with the Fe/Mo ratio. The maximum evaluated value for these ratios in the AMF series was lower than the small-

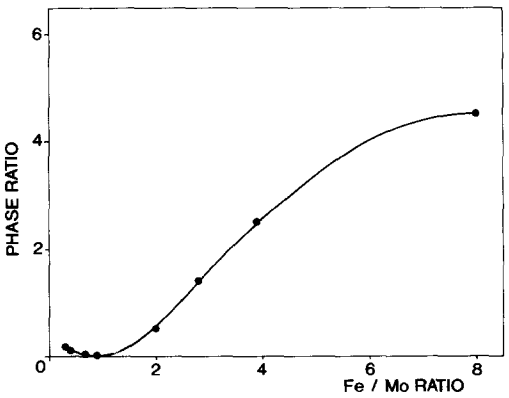

FIG. 2. Variation of the phase ratio.

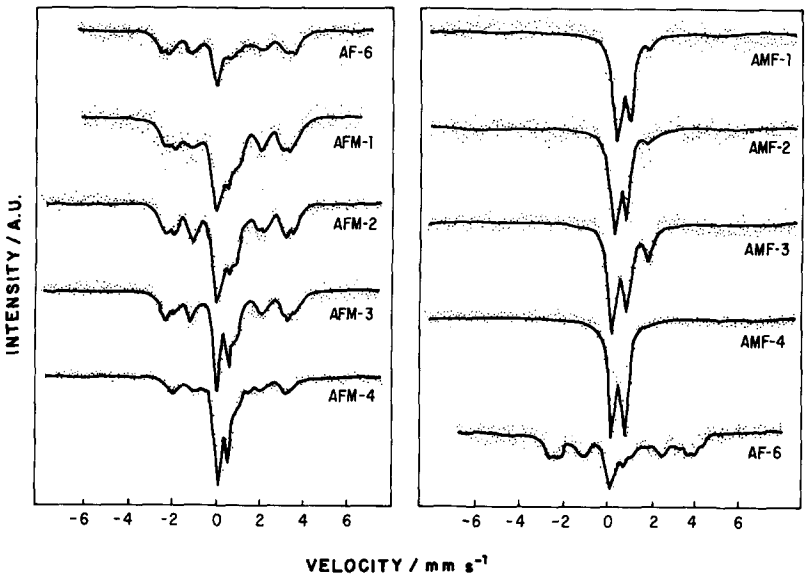

FIG. 3. Mössbauer spectra of catalysts (··· experimental data; —fitted data).

est observed for the AFM series. This seems to indicate that the impregnation of Mo before Fe favors the formation of phase 2.

The X-ray diffraction patterns of the sulfided catalysts were very weak. The main features of the patterns of the AFM catalysts could be assigned to pyrrhotite. MoS_2 was observed on the AMF catalysts. Some other lines (showing the same *d*-spacing) were present in all patterns. Although the *d*-values were imprecise (weak and broad lines) they would not be assigned to any known sulfide (or oxide or oxysulfide) of Fe or Mo,

TABLE 4

Mössbauer Parameters for Sulfided AMF Catalysts

Catalyst	Number of lines	IS (mm s^{-1})	QS (mm s^{-1})	H (kG)	Concentration (%)
AMF-1	2	0.23	0.94	0	88
	2	0.84	2.47	0	12
AMF-2	2	0.23	0.94	0	90
	2	0.84	2.47	0	10
AMF-3	2	0.23	0.94	0	95
	2	0.84	2.47	0	5
AMF-4	2	0.23	0.94	0	100
AF-6	2	0.32	0.91	0	17
	2	0.51	1.35	0	8
	2	1.22	2.10	0	11
	6	0.35	0.00	302	24
	6	0.37	0.16	256	32
	6	0.27	0.23	226	8

Note. IS, Isomer shift; QS, quadrupole splitting, and H, magnetic field.

TABLE 5

Mössbauer Parameters for Sulfided AFM Catalysts

Catalyst	Number of lines	IS (mm s^{-1})	QS (mm s^{-1})	H (kG)	Concentration (%)
AF-6	2	0.32	0.91	0	17
	2	0.51	1.35	0	8
	2	1.22	2.10	0	11
	6	0.35	0.00	302	24
	6	0.37	0.16	256	32
	6	0.27	0.23	226	8
AFM-1	2	0.32	0.91	0	10
	2	1.22	2.10	0	30
	6	0.43	0.00	302	23
	6	0.48	0.16	256	32
	6	0.57	0.23	226	5
AFM-2	2	0.32	0.91	0	29
	2	1.22	2.10	0	10
	6	0.61	0.00	302	19
	6	0.56	0.16	256	29
	6	0.58	0.23	226	7
AFM-3	2	0.32	0.91	0	34
	2	1.22	2.10	0	8
	6	0.54	0.00	302	19
	6	0.54	0.16	256	30
	6	0.59	0.23	226	9
AFM-4	2	0.32	0.91	0	57
	2	1.22	2.10	0	10
	6	0.83	0.00	302	9
	6	0.63	0.16	256	17
	6	0.61	0.23	226	7

suggesting the possible presence of a mixed Fe–Mo sulfide.

We could, as a first approach, suggest that the α- or γ-iron oxides gave rise to the pyrrhotite phase Fe_7S_8 while the iron molybdate type phase might form the mixed sulfide.

Mössbauer Spectroscopy

The Mössbauer spectra of the FeMo sulfided catalysts are illustrated in Fig. 3; for the sake of clarity the detailed subspectra have been omitted in the figure, although the spectroscopic parameters have been summarized in Tables 4 and 5 for the AMF and AFM catalysts, respectively. The isomer shift was referred to the source used (^{57}Co in Pd). A sulfided Fe/Al_2O_3 (AF-6) catalyst has been included as a reference to facilitate the comparison of the effects of the presence of a second metal.

Observation of the spectra of the AF-6 and of the AFM catalysts first confirms the presence of the pyrrhotite phase. According to the literature (*12*), this line-line spectrum is formed by three subspectra due mainly to the different arrangement of Fe vacancies throughout the lattice. Our fitted parameters are in perfect agreement with those reported by Morice *et al.* (*12*). The subspectra parameters were constant through the series although the proportion among them was different.

The central peaks of the spectrum obtained for the sulfided AF-6 catalyst could be fitted to three central doublets with quadrupole splitting of 0.91, 1.35 and 2.10 mm

s^{-1}, and an isomer shift of 0.32, 0.51 and 1.22 mm s^{-1}, respectively. The first doublet (QS = 0.91 mm s^{-1} and IS = 0.32 mm s^{-1}) could be assigned to Fe^{2+} low spin (octahedral coordination) according to Goodenough and Fatseas (*13*). This type of Fe has not been observed in any of its crystalline sulfides, so we are inclined to associate it with an amorphous non-stoichiometric sulfide phase.

Yagnik and Mathur (*14*) recorded the Mössbauer spectrum of the Fe(II) spinel ($FeAl_2O_4$), which presented two doublets with QS of 1.4 and 2.7 mm s^{-1} and IS of 0.80 and 1.4 mm s^{-1}. The first doublet was assigned to tetrahedral Fe sites (QS = 1.4 mm s^{-1}, IS = 0.8 mm s^{-1}), while an octahedral coordination was considered for the second (QS = 2.7 mm s^{-1}, IS = 1.4 mm s^{-1}). Hence, we could suppose that in our AF-6 catalyst the Fe(II) spinel was present with the Fe ions occupying both tetrahedral and octahedral coordinations. The population of each coordination was found to be similar. Although the iron aluminate phase is most likely to be crystalline it was not observed in our XRD patterns, probably due to its very low concentration (less than 10% of the total iron content or less than 1 wt%). This fact reflects one of the advantages of using Mössbauer spectroscopy as a characterization technique.

Besides the pyrrhotite spectrum the AFM spectra showed two central peaks that were able to be fitted into two doublets for all catalysts. They were fitted to the QS values of 0.9 and 2.1 mm s^{-1} and the IS values of 0.32 and 1.22 mm s^{-1}, respectively.

The interpretation of the Mössbauer spectra obtained from the studies of $FeMo_2S_4$ (*15, 16*) revealed that its crystal structure might be formed by two Fe^{2+} sites, which are independent crystallographically (*15*). The spectra could also be interpreted based on non-stoichiometric sites. For powder samples two central double peaks with IS of 0.72 and 0.66 mm s^{-1} and QS of 1.58 and 1.54 mm s^{-1} were found. These doublets were magnetic hyperfine split when the temperature was decreased (*16*), but the values of the spectroscopic hyperfine parameters were not reported. The values found for our spectra (IS of approximately 0.3 and 0.9 mm s^{-1} and QS of 0.9 and 2.0 mm s^{-1}) are too far from those of $FeMo_2S_4$ to be assigned to the presence of this stoichiometric mixed sulfide.

On the other hand, Mössbauer studies on mixed sulfides of iron and vanadium have indicated that the substitution of iron by vanadium reduced the interplanar spaces, but only slightly affected the intraplanar spaces (*17*). Moreover, V seems to stabilize the Fe^{2+} low-spin state (*13*). The parameters reported by Oka *et al.* (*17*) for the doublet found in FeV_2S_4 and FeV_4S_8 spectra have been used to conclude the presence of high-spin Fe^{2+} in the first compound (IS = 0.38 mm s^{-1}). Also, a transition to low spin could occur when temperature decreases. The IS of the second compound was 0.70 mm s^{-1} and it could be assigned to low-spin Fe^{2+}

The spectra obtained for AF-6 and AFM-2 sulfided catalysts at low temperatures are shown in Fig. 4. The AF-6 catalyst showed a magnetic hyperfine splitting when temperature was decreased; however, the fitted parameters were the same as those for room-temperature spectra. The low-temperature spectrum consequently indicates the presence of very small pyrrhotite particles whose spectrum intensity is increased when temperature is decreased.

This splitting was not observed for the FeMo catalyst, notwithstanding the small variation of the line intensities at the center of the spectra. Hence we might consider that both doublets presented by the AFM series correspond to two different Fe^{2+} species with different spin multiplicity. In view of this spin multiplicity difference caused by the presence of Mo, we might consider the possibilities of the Fe sites having different coordination such as that present on $FeMo_2S_4$. We could suggest that the features observed in the spectra are due to the presence of a mixed phase of non-stoichiometric type, like $Fe_xMo_yS_z$. In this com-

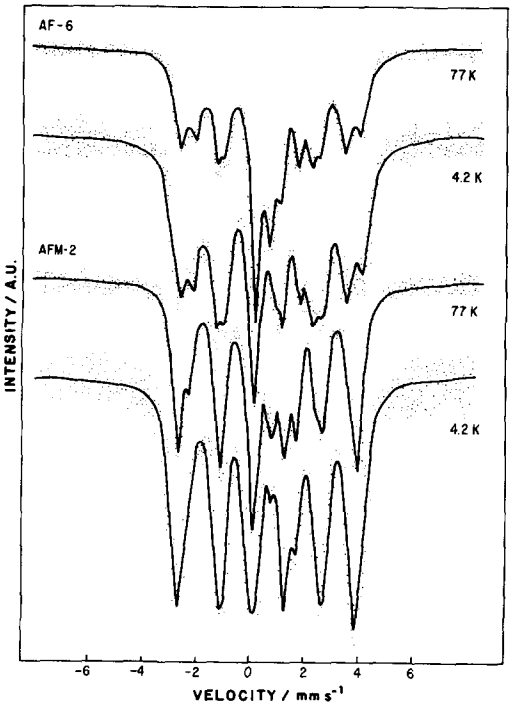

FIG. 4. Mössbauer spectra at low temperatures (··· experimental data; —fitted data).

pound, the amount and location of the substituted Mo in the lattice is such as to generate Fe^{2+} high-spin sites (IS $\approx$ 0.3–0.4) and Fe^{2+} low-spin sites (IS $\approx$ 0.8–1.3). The Fe coordination is more difficult to predict. The QS values fell in the range of those obtained for both Fe–Mo and Fe–V mixed sulfides. Thus, this compound might possess low symmetry, probably monoclinic, for which one iron site might correspond to tetrahedral coordination (I) and the other to octahedral coordination (II).

For the AMF series, only the two central doublets characteristic of I and II Fe sites were observed. These results indicate that the first impregnation of Mo inhibits the formation of pyrrhotites in the final catalysts.

The variation of the proportion of the different Fe species with the concentration of the second impregnated metal is presented in Fig. 5. The proportion of sites I increases and that of sites II decreases with the concentration of the second impregnated metal. For the AMF series, the formation of sites I was favored at the expense of sites II depletion. Meanwhile, in the AFM series for which pyrrhotites were observed, the formation of sites I occurred mainly due to pyrrhotite shortage. Since the first type of sites is believed to have a tetrahedral coordination while the second is supposed to be octahedral, the tetrahedral coordination seems to be most stable for this kind of catalyst.

The proportion of sites I exhibited for the AMF catalysts was much larger than that observed for the AFM series. The impregnation of Mo before Fe seems to favor the formation of a mixed Fe–Mo phase. In other words, once Mo is on the catalyst, the inter-

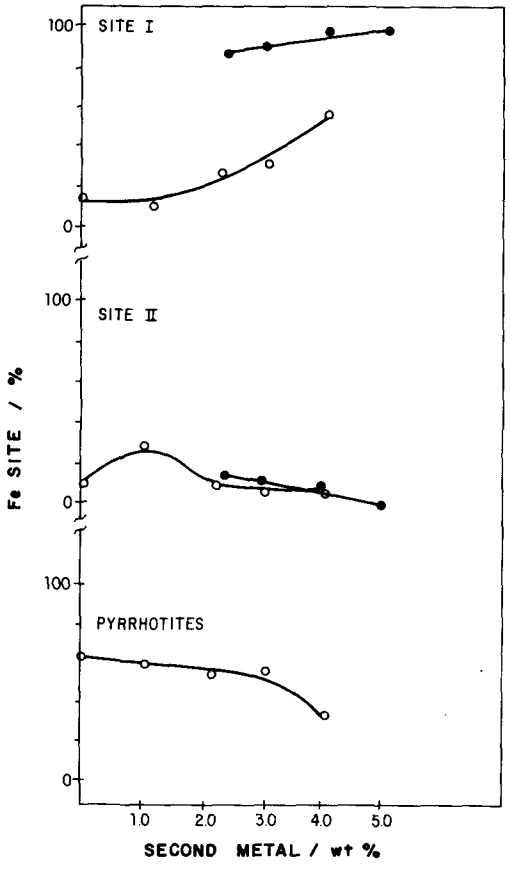

FIG. 5. Variation of Fe sites proportion. AFM (○); AMF (●).

action Fe–Mo seems to be greater than that of Fe support. For instance, the formation of iron aluminate was completely inhibited by the presence of Mo. Consequently, all the iron impregnated in the second step forms a mixed compound with the Mo impregnated in the first step. The formation of a sulfide phase of a single metal (iron) was observed in the cases where iron was impregnated first (AFM series). We report the effect of the structure and the nature of the catalytic phases on activity, selectivity, and stability in other publications (*7, 8*). In fact, from the catalytic standpoint, the FeMo-type catalysts of the present work behave rather differently than CoMo-type catalysts. In general, although CoMo catalysts are highly active, they are less stable, and their catalytic activity decays rapidly upon metal deposition during use. The FeMo catalysts instead are less active but possess a longer lifetime. Their stability seems to be related to the presence of an iron monosulfide phase (*7*). Typically in the case of CoMo-type catalysts the presence of Co monosulfide is undesirable.

CONCLUSIONS

The impregnation sequence and the Fe/Mo ratio is determinant for the final crystal composition of the studied catalysts.

For the precursor samples when Fe was impregnated in a first step the following phases were found: α-Fe_2O_3, γ-Fe_2O_3, and α-$FeMoO_4$. When Fe was impregnated in a second step the phases were the following: α-Fe_2O_3, α-$FeMoO_4$, and β-$FeMoO_4$. In the sulfided catalysts the phases present were: Fe_7S_8 and $Fe_xMo_yS_z$. The ratio among the two phases of the sulfided catalysts (containing Fe and Fe + Mo) changes with the Fe/Mo ratio.

By means of Mössbauer spectroscopy we have found different types of Fe sites in the catalysts. When Fe was impregnated in the second step, iron sulfide in the form of pyrrhotite was not observed. All the sulfided catalysts presented two sites of Fe^{2+} (I and II) that corresponded to the $Fe_xMo_yS_z$ phase. The proportion of these sites depends on the concentration of the second impregnated metal. Sites of type I have tetrahedral coordination, while those of type II have octahedral coordination. Increase of the Mo concentration on the Fe/Al_2O_3 catalyst causes a decrease of pyrrhotite formation upon sulfidation.

REFERENCES

1. Delmon, B., *Am. Chem. Soc. Div. Pet. Chem. Prep.* **22,** 503 (1977).
2. Oleck, S. M., and Sherry, H. S., *Ind. Eng. Chem. Process Des. Dev.* **16,** 525 (1977).
3. Nakamura, M., Togari, O., and Ono, T., *in* "45th API Ref. Meet.," Vol. 32, p. 201, 1980.
4. Arias, B., Kum, H., and Galiasso, R., US Patent, 4,499,202.
5. Ramirez de Agudelo, M. M., and Galarraga, C., *Rev. Soc. Venez. Catal.* **5,** (1991).
6. Ramirez de Agudelo, M. M., and Galarraga, C., US Patent, 4,729,980.
7. Ramirez de Agudelo, M. M., and Galarraga, C., *J. Chem. Eng.* **46,** 61 (1991).
8. Galarraga, C., and Ramirez de Agudelo, M. M., *Rev. Tec. INTEVEP* **10,** 2 (1991).
9. Topsøe, H., Clausen, B. S., and Mørup, S., *Hyper. Inter.* **27,** 231 (1986).
10. Mørup, S., Clausen, B. S., and Topsøe, H., *J. Phys.* **40,** C2-88 (1979).
11. Topsøe, H., Clausen, B. S., Candia, R., Wivel, C., and Mørup, S., *Bull. Soc. Chim. Belg.* **90,** 12 (1981).
12. Morice, J. A., Rees, L. V. C., and Rickard, D. T., *J. Inorg. Nucl. Chem.* **31,** 3797 (1969).
13. Goodenough, J. B., and Fatseas, G. A., *J. Solid State Chem.* **41,** 1 (1982).
14. Yagnik, C. K., and Mathur, H. B., *J. Phys. C.* **2,** 469 (1968).
15. Abe, M., Kaneta, K., and Uchino, K., *J. Phys. Soc. Jpn.* **44,** 1739 (1978).
16. Fatseas, G. A., Meury, J. L., and Varret, F., *J. Phys. Chem. Solids* **42,** 239 (1981).
17. Oka, Y., Kosuge, K., and Kachi, S., *Mater. Res. Bull.* **12,** 1117 (1977).